2014 IEEE Congress on Evolutionary Computation (CEC)
July 6-11, 2014, Beijing, China

Many-objective evolutionary computation for optimization of separated-flow control using a DBD plasma actuator

Takeshi Watanabe, Tomoaki Tatsukawa, Antonio López Jaimes, Hikaru Aono,
Taku Nonomura, Akira Oyama, and Kozo Fujii
Japan Aerospace Exploration Agency
Institute of Space and Astronautical Science
3-1-1 Yoshinodai, Chuo-ku, Sagamihara, Kanagawa, 252-5210, Japan
Email: watanabe@flab.isas.jaxa.jp

***Abstract*—In this paper, an algorithm for many-objective evolutionary computation, which is based on the NSGA-II with the Chebyshev preference relation, is applied to multi-objective design optimization problem of dielectric barrier discharge plasma actuator (DBDPA). The present optimization problem has four design parameters and six objective functions. The main goal of the paper is to extract useful design guidelines to predict control flow behavior based on the DBDPA parameter values using the resulting approximation Pareto set obtained by the optimization.**

I. Introduction

Multi-objective design exploration[1] is an approach to extract useful design guidelines from non-dominated solutions obtained by evolutionary multi-objective optimization (EMO). This approach has been successfully demonstrated in many practical design problems[2][3].

Although Pareto-based multi-objective evolutionary algorithms (MOEAs), have been widely applied to solve real-world applications (for example, NSGA-II[4] or SPEA2[5]), it is known that their convergence performance is less effective in optimization problems with more than four objectives (called many-objective optimization problems)[6]. Thus, many scalability studies have been conducted recently (see e.g., [7], [8], [9]) and some proposals to deal with a large number of objectives have proposed as well (see e.g, [10], [11], [12], [13]).

In this paper we consider the following many-objective aerodynamical problem with six objective functions. These objective functions concern the improvement of aerodynamical properties of an airfoil by use of a dielectric barrier discharge plasma actuator (DBDPA)[14] which is put on the airfoil. DBDPA is one of the options to control flows around an airfoil. Besides an airfoil separation control using the DBDPA has attracted great interest[15][16][17] in the last decade. This device controls the global flow field by adding the small disturbance on local small region in order to suppress the separation.

From the aerodynamical point of view, a separation control of an airfoil is important to control aircraft. When an angle of attack (AoA) is small enough the lift of the airfoil is proportional to the AoA. However when the AoA exceeds a specified value, the lift suddenly drops because the flow separates from the surface of the airfoil and the nature of the flow changes. This phenomenon is called "stall" and the smallest AoA where the flow separates is called "stall angle". If we can increase the stall angle by controlling flow around the airfoil, we can obtain larger lift by using the same airfoil. For example stall angle of NACA 0015, which is the airfoil used in the present study, is about $10°$[18], however separation can be suppressed and then the stall angle becomes larger at least $16°$ if we can choose an appropriate control parameters using a DBDPA as shown in this paper.

The DBDPA consists of two electrodes and a dielectric as shown in Fig. 1. It generates plasma by means of the DBD in the area between the exposed electrode and the dielectric when a high alternating current (AC) voltage is applied to the electrodes and flow is induced over an actuator.

The performance of separation control strongly depends on control parameters of DBDPA such as an input energy, a burst frequency, an installation location and so on. Thus, parametric studies for these parameters have been recently conducted[17], however, it is still difficult to find out "good"

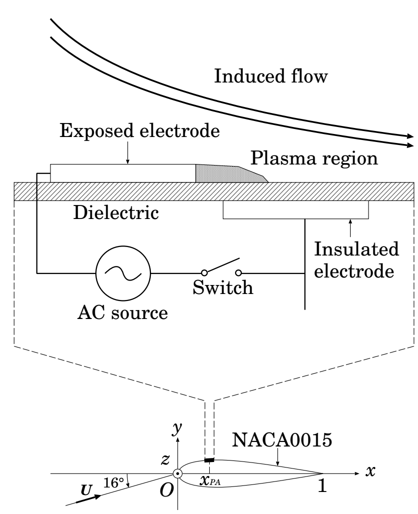

Fig. 1. Configuration of DBDPA. Switch is used to generate burst wave as shown in Fig. 3.

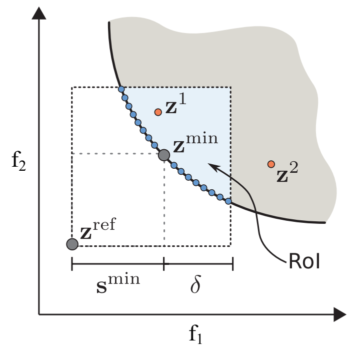

Fig. 2. Non-dominated solutions with respect to the Chebyshev preference relation.

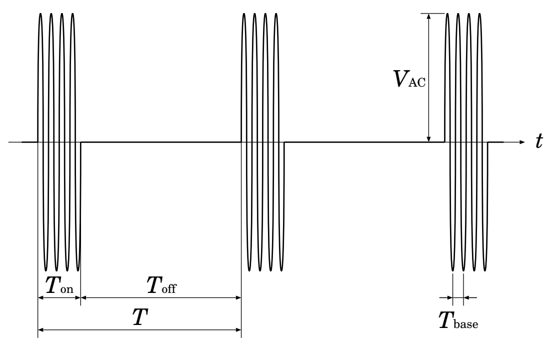

Fig. 3. Definitions of F^{+} and BR, where $F^{+} = 1/T$ and $BR = T_{\rm on}/T$. On-off procedures are repeated time-periodically using the switch shown in Fig. 1 so as to save the power consumption.

parameter combinations because they exponentially increase with respect to the number of parameters. Further flow control becomes more difficult when the AoA becomes larger. In a case when the AoA is slightly larger than the stall angle, flow is made to attach to the airfoil easier while it becomes more difficult when the AoA becomes larger because the flow becomes so called “deep stall” or “massive separation”. The present case, AoA equals $16°$, corresponds to the “deep stall” and thus “good” parameter range becomes narrower. If the aimed parameter range is narrower, we should calculate more combinations of parameters and thus it is difficult to apply parametric search.

Therefore a more efficient procedure to find such a combination is necessary and evolutionary algorithm is one of the candidates. In the present problem there are many optimization objectives for practical use such as lift increase, drag reduction, energy consumption reduction, robustness, and so on. In the present case we have six objective functions. In order to obtain an approximation of the Pareto front for this problem we have adopted an algorithm using the Chebyshev preference relation embedded in NSGA-II (NSGA-II-Cheby)[10]. We have selected this algorithm because it has been shown a good performance in many-objective problems (see e.g, [10], [19]).

There is another difficulty when Reynolds number is high because the higher the Reynolds number is, the smaller the spatial and temporal structure of the fluid motion become and thus larger resolution is required to solve the flow field. In the present case the number of grid points of the calculation is 2×10^7 to resolve the flow field, which requires large calculation resources even for a single calculation. Further we need to calculate many cases to proceed the iteration of evolutionary computation and then the cost of the total calculation in the present study is very large. Such the calculation becomes possible by using K-computer.

The main contribution of the paper is to provide design guidelines in flow control using a DBDPA. The guidelines are extracted from the resulting approximation Pareto front obtained by NSGA-II-Cheby. Although the Pareto optimal front for this problem is not known, the trend of the hypervolume obtained at each generation suggests that the achieved trade-off solutions represent a good approximation of the true Pareto front.

II. Evolutionary computation: NSGA-II-Cheby

NSGA-II-Cheby is applied to conduct the present multi-objective design problem optimization. Recent studies[7][8][9] have concluded that EMO algorithms based on Pareto dominance scale poorly with respect to the number of objectives. For solving many-objective optimization problem of the DBDPA design parameters, we have adopted the Chebyshev preference relation, which is a recently proposed relation[10] to handle more than three objectives.

For the sake of completeness, in the following we briefly describe NSGA-II-Cheby algorithm. However, the interested reader is referred to [10] for further details.

First, we define a region of interest (RoI) with respect to a given reference point $\boldsymbol{z}^{\rm ref}$ as shown in Fig. 2. The RoI comprise solutions with an achievement value

$$s(\boldsymbol{z}|\boldsymbol{z}^{\rm ref}) \leq s^{\rm min} + \delta,$$

where $s^{\rm min}$ is the best achievement value found in the population, δ is a threshold that determines the size of the RoI, and $s(\boldsymbol{z}|\boldsymbol{z}^{\rm ref})$ is defined by the Chebyshev achievement function

$$\begin{aligned} s(\boldsymbol{z}|\boldsymbol{z}^{\rm ref}) &= \max_{i=1,\ldots,k} \{\lambda_i (z_i - z_i^{\rm ref})\} \\ &\quad + \rho \sum_{i=1}^{k} \lambda_i (z_i - z_i^{\rm ref}), \end{aligned} \tag{1}$$

where $\boldsymbol{z}^{\rm ref}$ is a reference point, $\boldsymbol{\lambda} = \{\lambda_i\}$ is a vector of weights such that $\forall i\ \lambda_i \geq 0$ and, for at least one i, $\lambda_i > 0$, and $\rho > 0$ is a sufficiently small augmentation coefficient. Further the ϵ-fitness function $F_\epsilon(\boldsymbol{z}^1)$ is introduced as

$$F_\epsilon(\boldsymbol{z}^1) = \sum_{\boldsymbol{z}^2 \in P \setminus \{\boldsymbol{z}^1\}} - \exp\left[-I_\epsilon(\{\boldsymbol{z}^2\}, \{\boldsymbol{z}^1\})/(c \cdot \kappa)\right], \tag{2}$$

where P is the current population, c is a normalizing factor given by $c = \max_{\boldsymbol{z}^1, \boldsymbol{z}^2 \in P} |I_\epsilon(\{\boldsymbol{z}^2\}, \{\boldsymbol{z}^1\})|$, κ is a scaling factor that regulates the influence of the dominating solutions over dominated ones, which is set to be $\kappa = 0.05$ as recommended by Zitzler et al.[20], and I_ϵ is the additive ϵ-indicator defined by

$$\begin{aligned} & I_\epsilon(A, B) \\ &= \inf_{\epsilon \in \mathbb{R}} \left\{ \forall \boldsymbol{z}^2 \in B, \exists \boldsymbol{z}^1 \in A : z_i^1 \leq \epsilon + z_i^2, i = 1, \cdots, k \right\}. \end{aligned}$$

Solutions in the RoI are compared using Eq. (2), while solutions outside of the RoI are compared using Eq. (1) as follows: A solution $\boldsymbol{z}^1$ is preferred to solution $\boldsymbol{z}^2$ when

TABLE I. PARAMETER VALUES FOR THE COMPUTATION.

Parameter	Value
Population size	52
Number of generations	15
Crossover rate	0.9
Mutation rate	1/4
Crossover index	30
Mutation index	20
RoI size	0.9

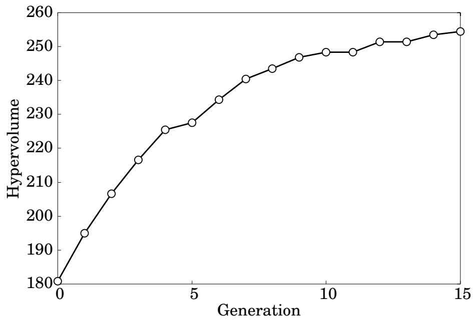

Fig. 4. Hypervolume of the approximation Pareto set for each generation.

- $\boldsymbol{z}^1, \boldsymbol{z}^2 \notin$ RoI and $s(\boldsymbol{z}^1|\boldsymbol{z}^{\mathrm{ref}}) < s(\boldsymbol{z}^2|\boldsymbol{z}^{\mathrm{ref}})$,

  or
- $\boldsymbol{z}^1, \boldsymbol{z}^2 \in$ RoI and $F_\epsilon(\boldsymbol{z}^1) > F_\epsilon(\boldsymbol{z}^1)$,

  or
- $\boldsymbol{z}^1 \in$ RoI and $\boldsymbol{z}^2 \notin$ RoI.

III. DEFINITION OF THE DESIGN PROBLEM

We consider a NACA 0015 airfoil which is put in a uniform flow as shown in Fig. 1. The AoA of the airfoil was set to $\alpha = 16^\circ$ in order to consider a case with massive separation.

The DBDPA is put on the airfoil to control the separation with the following four design parameters:

- Non-dimensional plasma scale parameter D_C: $D_C \in \{D_{Ci} | D_{Ci} = i, i \in \mathbb{Z} \cap [1, 160]\}$,
- Burst ratio BR: $BR \in \{BR_i | BR_i = 0.05i, i \in \mathbb{Z} \cap [1, 20]\}$,
- Burst frequency F^+: $F^+ \in \{F_i^+ | F_i^+ = 0.5i, i \in \mathbb{Z} \cap [1, 40]\}$,
- Installation location x_{PA}: $x_{PA} \in \{x_i | x_i = i \times 10^{-3}, i \in \mathbb{Z} \cap [0, 300]\}$,

where $F^+ = 1/T$ and $BR = T_{\mathrm{on}}/T$. Definitions of T and T_{on} are shown in Fig. 3. Note that period of the AC source T_{base} is small enough compared to T_{on}.

Six objective functions are taken into account as follows:

- Mean lift coefficient $\overline{C_L(t)}$ (maximize),
- Mean drag coefficient $\overline{C_D(t)}$ (minimize),
- D_C (minimize),
- $D_C \times BR$ (minimize),
- Standard deviation of $C_L(t)$, $C_{L,dev}$ (minimize),
- Standard deviation of $C_D(t)$, $C_{D,dev}$ (minimize),

where C_L, and C_D denotes lift coefficient, and drag coefficient, respectively. C_L and C_D are taken into account to improve the performance of the airfoil whereas D_C and BR, to reduce the energy consumption because we want to enhance the performance of the airfoil using as low energy consumption as possible.

Flow fields are solved using LANS3D[21][22], a three-dimensional fluid solver developed at the ISAS/JAXA, with 2×10^7 grid points. The computational cost per capita is 3.88×10^3 [node·hour] on the K-computer and thus the total cost is about 3.2×10^6 [node·hour]. Six objective values are obtained by results of calculations. See also reference [17] for details of the calculations.

NSGA-II-Cheby algorithm was applied to obtain a representative sample of the Pareto front of the above defined design problem. Parameter values for the NSGA-II-Cheby are shown in Table I. The number of generation is not very large due to the computational cost, however, convergence of the hypervolume is confirmed to be relevant as shown in Fig. 4.

IV. RESULTS

Outline of the approximated Pareto front is shown in Fig. 5. Because the original set of non-dominated solutions is embedded in six dimensional space, it is very difficult to imagine the shape of the approximated Pareto front. However, because our aim of this study is to extract "useful" information from the solution set, it is not necessary to understand the "exact shape" of the front, but to extract a "safe region" of the design parameters. From this point of view, the most important task is to classify the objective-value space by the design-parameter space.

Non-dominated solutions are classified into three types A, B, and C in the objective-function space as shown in Fig. 6. Definitions of these three types are given as follows:

A: In this type, flow is well controlled with respect to C_L, C_D, $C_{L,dev}$, and $C_{D,dev}$. In this type a positive trade-off between $D_C \times BR$ and C_L/C_D exists as shown in Fig. 7 and thus we can choose many options between energy consumption and performance improvement.

B: In this type, although C_L is improved, both C_D and $C_{D,dev}$ becomes worse. The typical characteristic is shown in the right-top quarter of the center panel of Fig. 6.

C: In this type, flow is not controlled enough. However many solutions in this type tend to have small D_C as shown in Fig. 8 and Fig. 9.

Typical flow pattern in each region is shown in Fig. 10.

Next, we analyze the design-parameter space because our aim is to predict the flow type in advance, i.e., only from information of design parameters. Figure 8 shows the dependency of the flow type with respect to F^+ and D_C. Flow field is predicted by F^+ and D_C as follows.

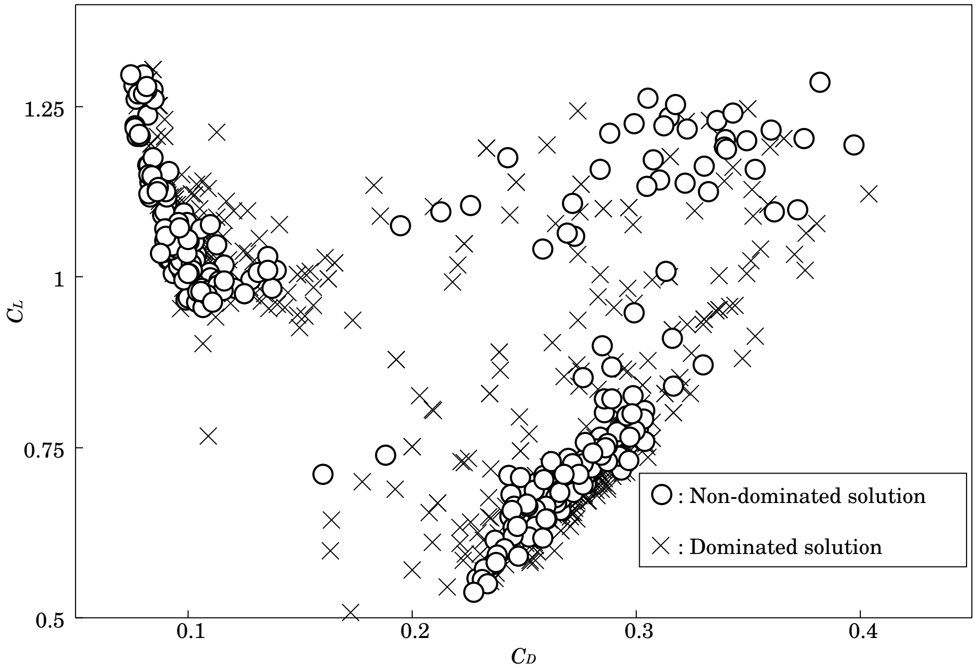

Fig. 5. Projection of the result onto the C_L-C_D plane. “X” denotes dominated solutions, and “○”, non-dominated solutions, respectively.

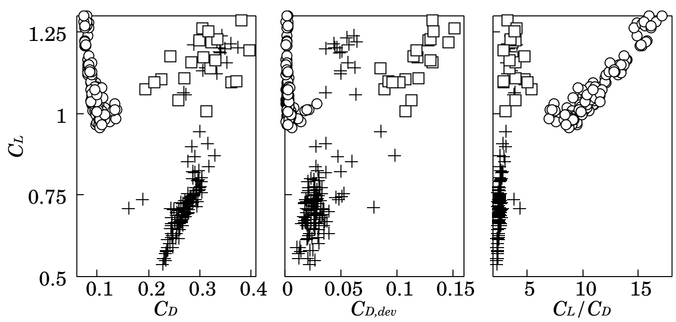

Fig. 6. Projection of the set of non-dominated solutions onto, from left to right, the C_D-C_L plane, $C_{D,dev}$-C_L plane, and C_L/C_D-C_L plane, respectively. In the figures, ◯ denotes “type A”, □, “type B”, and +, “type C”, respectively.

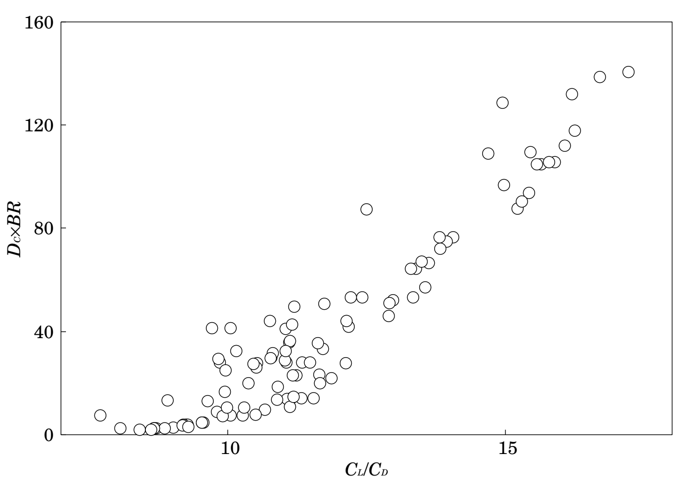

Fig. 7. Type A solutions extracted using the branch diagram. We can choose many options considering the trade-off relationship between energy reduction (reduce $D_C \times BR$) and the performance of the airfoil (increase C_L/C_D).

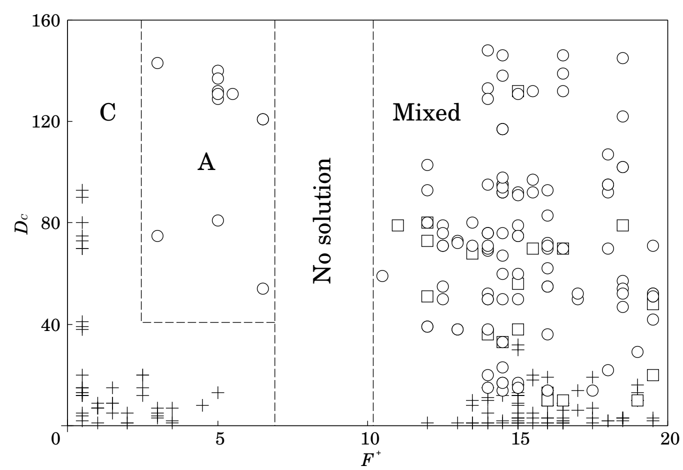

Fig. 8. Projection of the set of non-dominated solutions onto the F^+-D_C plane. As in Fig. 6, ◯ denotes “type A”, □, “type B”, and +, “type C”, respectively. Each region is characterized as follows. C: $0.5 \leq F^+ \leq 2.5$ or $3 \leq F^+ \leq 6.5$ and $D_C \leq 13$. A: $3 \leq F^+ \leq 6.5$ and $D_C \geq 54$. No solution: $7 \leq F^+ \leq 10$. Mixed: $F^+ \geq 10.5$.

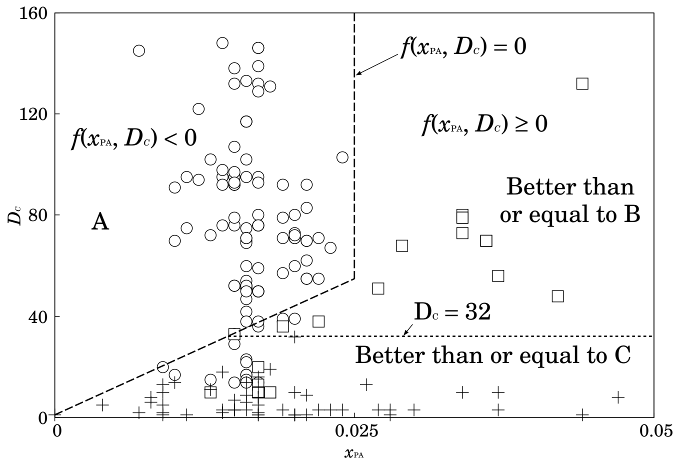

Fig. 9. Projection of the subset, "Mixed" region in Fig. 8, of non-dominated solutions onto the x_{PA}-D_C plane. As in Fig. 6, ◯ denotes "type A", □, "type B", and $+$, "type C", respectively. "Safe side" is extracted by a threshold function $f(x_{PA}, D_C)$ with a slight compensation of type A, and B.

C: $0.5 \leq F^+ \leq 2.5$ or $3 \leq F^+ \leq 6.5$ and $D_C \leq 13$,
A: $3 \leq F^+ \leq 6.5$ and $D_C \geq 54$,
No solution: $7 \leq F^+ \leq 10$,
Mixed: $F^+ \geq 10.5$.

In this classification, we can not distinguish the solution type in "Mixed" region and thus other thresholds are required.

Figure 9 shows appropriate thresholds to classify the "mixed" region using D_C and x_{PA}. This projection shows that although flow pattern is sensitive to both D_C and x_{PA} when $D_C \leq 32$, the relationship among them becomes much clear when $D_C > 32$. From the engineering point of view, such sensitive region is not chosen in terms of robustness of the design and thus it is enough to classify the region from the "safe side". That is to say, the nature of a classified region is determined by the individual which has the worst property. Then the region "Better than or equal to B" is safely classified into B, and "Better than or equal to C", C. Therefore threshold is given by a function $f(x_{PA}, D_C)$ defined as

$$f(x_{PA}, D_C) = \begin{cases} 2134x_{PA} + 1 - D_C & (x_{PA} < 0.025) \\ x_{PA} - 0.025 & (x_{PA} \geq 0.025) \end{cases} .$$

Using this threshold, flow is always type A when $f(x_{PA}, D_C) < 0$. For the rest of the region, contained solutions are at worst type B when $D_C > 32$.

This classification in design-parameter space is very important because we can approximately choose aimed performance in advance as sufficient conditions.

In sum, resulting flow patterns controlled by DBDPA are classified into three types according to the following branch diagram:

- $F^+ \leq 6.5$
  - $F^+ \geq 3$ and $D_C \geq 54$: A.
  - Others: C.
- $7 \leq F^+ \leq 10$: No solution.
- $F^+ \geq 10.5$
  - $f(x_{PA}, D_C) \geq 0$
    - $D_C > 32$: B.
    - $D_C \leq 32$: C.
  - $f(x_{PA}, D_C) < 0$: A.

This information is useful to design flow control using DBDPA.

Using this branch diagram, type A solutions are extracted as shown in Fig. 7. This figure shows that when $C_L/C_D \lesssim 12$, we can increase C_L/C_D with small amount of increase of $D_C \times BR$, however when C_L/C_D exceeds that point, the slope of the front becomes steeper and we need more input energy to increase C_L/C_D. In type A solution set, we can choose many options considering the trade-off relationship between energy reduction ($D_C \times BR$ decreases) and the performance of the airfoil (C_L/C_D increases).

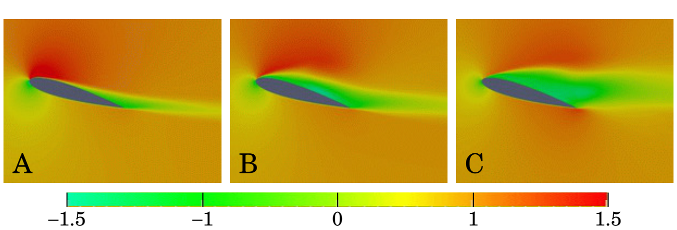

Fig. 10. Typical flow pattern of each type. Background color is the magnitude of the x-component of the normalized, time- and spanwise-averaged flow field.

V. Conclusions

Optimization of running parameters of dielectric barrier discharge plasma actuator (DBDPA) with six objective functions using NSGA-II with the Chebyshev preference relation (NSGA-II-Cheby) is conducted to obtain useful design guidelines for separated-flow control for NACA 0015 which angle of attack (AoA) is 16°.

The multi-objective formulation of the DBDPA problem proved to be an excellent tool to extract useful information about the problem since we were able to determine a branch diagram for guidelines for control flow.

First, flow patterns are classified into three regions, A, B, and C, with respect to the objective values. In Type A region, flow is well controlled with respect to C_L, C_D, $C_{L,dev}$, and $C_{D,dev}$. Separation is enough suppressed as shown in the left panel of Fig. 10. In this region the larger $D_C \times BR$ is, the larger C_L becomes and the smaller C_D becomes and thus, the larger C_L/C_D becomes. Therefore we have many options considering the positive trade-off between $D_C \times BR$ and C_L/C_D as shown in Fig. 7. For type B region, although C_L is improved, both C_D and $C_{D,dev}$ becomes worse. Although separation is relatively suppressed compared to type C, that is not enough as shown in the center panel of Fig. 10. For type C region, flow is not controlled enough as shown in the right panel of Fig. 10.

Next, corresponding region in the design-parameter space is analyzed. The most sensitive parameter for flow control is burst frequency F^+. When $F^+ \leq 6.5$, type A and C are well separated with respect to F^+ and D_C as shown in Fig. 8. On the other hand, when $F^+ \leq 10.5$, resulting objective values are sensitive to the installation location x_{PA} and non-dimensional plasma scale parameter D_C as shown Fig. 9. In this case the relationship between design parameters and the flow type is complicated when D_C is small. Therefore, from the engineering point of view, thresholds are set from the safe side and three types are separated approximately, however is well approximated as shown in Fig. 9.

Finally the relationship between the regions in design-parameter space and objective-value space are incorporated into the branch diagram and a simple and useful knowledge is extracted from complicated six-dimensional set of non-dominated solutions.

ACKNOWLEDGMENT

Part of the results is obtained by using the K computer at the RIKEN Advanced Institute for Computational Science (Proposal number hp130030). This research is partially supported by Strategic Program for Innovative Research (SPIRE) of High Performance Computing Initiative (HPCI) (Proposed numbers of hp130030 and hp130001). The authors would like to thank Dr. M. Sato and Dr. A. Yakeno for helpful comments and discussions.

REFERENCES

[1] S. Obayashi, S.Jeong, and K. Chiba, "Multi-objective design exploration for aerodynamic configurations," *IAAA-2005-4666*, 2005.

[2] K. Chiba, A. Oyama, S. Obayashi, K. Nakahashi, and H. Morino, "Multidisciplinary design optimization and data mining for transonic regional-jet wing," *Journal of Aircraft*, vol. 4, pp. 1100–1112, 2007.

[3] A. Oyama, T. Nonomura, and K. Fujii, "Data mining of pareto-optimal transonic airfoil shapes using proper orthogonal decomposition," *IAAA-2009-4000*, 2009.

[4] K. Deb, A. Pratap, S. Agarwal, and T. Meyarivan, "A fast and elitist multiobjective genetic algorithm: Nsga-ii," *IEEE Transactions on Evolutionary Computation*, vol. 6, no. 2, pp. 182–197, April 2002.

[5] E. Zitzler, M. Laumanns, and L. Thiele, "Spea2: Improving the strength pareto evolutionary algorithm for multiobjective optimization," *Evolutionary Methods for Design, Optimisation and Control with Application to Industrial Problems, Proceedings of the EUROGEN2001 Conference*, pp. 95–100, 2002.

[6] R. C. Purshouse and P. J. Fleming, "Evolutionary many-objective computation: An exploratory analysis," *Proceedings of the IEEE Congress on Evolutionary Computation, CEC 2003*, vol. 3, pp. 2066–2073, 2003.

[7] H. Ishibuchi, N. Tsukamoto, and Y. Nojima, "Evolutionary many-objective optimization: A short review," *CEC'2008*, pp. 2424–2431, 2008.

[8] T. Wagner, N. Beume, and B. Naujoks, "Pareto-, aggregation-, and indicator-based methods in many-objective optimization," *EMO 2007*, pp. 742–756, 2007.

[9] J. Knowles and D. Corne, "Quantifying the effects of objective space dimension in evolutionary multiobjective optimization," *EMO 2007*, pp. 757–771, 2007.

[10] A. López Jaimes, C. A. Coello Coello, A. Oyama, and K. Fujii, "An alternative preference relation to deal with many-objective optimization problems," *Evolutionary Multi-Criterion Optimization*, pp. 291–306, 2013.

[11] Q. Zhang and H. Li, "Moea/d: A multiobjective evolutionary algorithm based on decomposition," *IEEE Transactions on Evolutionary Computation*, vol. 11, pp. 712–731, 2007.

[12] J. Bader and E. Zitzler, "Hype: An algorithm for fast hypervolume-based many-objective optimization," *Evol. Comput.*, pp. 45–76, 2011.

[13] K. Deb and H. Jain, "An evolutionary many-objective optimization algorithm using reference-point based non-dominated sorting approach, part i: Solving problems with box constraints," *Evolutionary Computation, IEEE Transactions on*, p. 1, 2013.

[14] T. C. Corke, M. L. Post, and D. M. Orlov, "Sdbd plasma enhanced aerodynamics: concepts, optimization and applications," *Progress in Aerospace Sciences*, vol. 43, pp. 193–217, 2007.

[15] M. L. Post and T. C. Corke, "Separation control on high angle of attack airfoil using plasma actuators," *AIAA Journal*, vol. 42, no. 11, pp. 2177–2184, 2004.

[16] T. C. Corke, C. L. Enloe, and S. P. Wilkinson, "Dielectric barrier discharge plasma actuators for flow control," *Annual Review of Fluid Mechanics*, pp. 505–529, 2010.

[17] M. Sato, K. Okada, T. Nonomura, H. Aono, A. Yakeno, K. Asada, Y. Abe, and K. Fujii, "Massive parametric study by les on separated-flow control around airfoil using dbd plasma actuator at reynolds number 63,000," *Proceedings of 43rd AIAA Fluid Dynamics Conference and Exhibit*, pp. 24–27, June 2013.

[18] T. Nonomura, H. Aono, M. Sato, A. Yakeno, K. Okada, Y. Abe, and K. Fujii, "Control mechanism of plasma actuator for separated flow around naca0015 at reynolds number 63,000 —separation bubble related mechanisms—," *AIAA-2013-0853*, 2013.

[19] A. Lopez Jaimes, A. Oyama, and K. Fujii, "Space trajectory design: Analysis of a real-world many-objective optimization problem," in *Evolutionary Computation (CEC), 2013 IEEE Congress on*. IEEE, 2013, pp. 2809–2816.

[20] E. Zitzler and S. Künzli, "Indicator-based selection in multiobjective search," *PPSN VIII*, pp. 832–842, 2004.

[21] K. Fujii, "Developing an accurate and efficient method for compressible flow simulations —example of cfd in aeronautics—," *The Proceedings: Fifth International Conference on Numerical Ship Hydrodynamics*, 1990.

[22] K. Fujii and S. Obayashi, "High-resolution upwind scheme for vortical-flow simulations," *Journal of Aircraft*, vol. 26, no. 12, pp. 1123–1129, 1989.